Deposition of Pectin/Poly-L-lysine Multilayers with Pectins of Varying Degrees of Esterification

Alina Krzeminski,[†] Mariya Marudova,[‡] Jonathan Moffat,[†] Timothy R. Noel,[†] Roger Parker,[†] Nikolaus Wellner,[†] and Steve G. Ring*[,†]

Institute of Food Research, Norwich Research Park, Colney, Norwich, NR4 7UA United Kingdom, and University of Plovdiv "Paisii Hilendarski", 24 Tsar Assen, 4000 Plovdiv, Bulgaria

Received September 28, 2005; Revised Manuscript Received November 28, 2005

The effect of pectin esterification on the assembly of multilayers consisting of poly-L-lysine (PLL) and pectin was studied using surface plasmon resonance (SPR), Fourier transform infrared−attenuated total reflection spectroscopy (FTIR-ATR), and a quartz crystal microbalance with dissipation monitoring (QCMD). With each layer deposited, there was a progressive increase in mass. The net charge of the multilayers was positive and increased with increasing degree of esterification of the pectin. Multilayer fabrication involved a limited fractionation of the pectin preparations, with the more highly esterified pectins having a weaker affinity for PLL. The multilayers were relatively hydrated structures with estimates of solids content in the range 10−32% w/w. The more highly esterified pectins had a tendency to form more hydrated structures, which showed a strong deswelling when PLL was added to a freshly deposited pectin layer.

Introduction

The attraction between oppositely charged polyelectrolytes can create a range of structures, including complexes,[1,2] coacervates,[3] networks, and multilayers.[4] Over the past decade, the layer-by-layer technique has been developed for the formation of multilayers through the sequential deposition of oppositely charged polymers.[5,6] A requirement for multilayer formation is that the addition of an oppositely charged polyelectrolyte to a charged surface results in charge reversal, normally depicted as charged loops and tails of the polyelectrolyte extending from the surface. Charge reversal permits successive deposition of oppositely charged polyelectrolytes. The multilayers formed are nonequilibrium structures. Although many studies have been performed with synthetic polyelectrolytes, there are fewer on the formation of multilayers using biopolyelectrolytes. Recent examples include alginate/poly-L-lysine,[7] hyaluronan/poly-L-lysine,[8] and hyaluronan/chitosan.[9] For these weak polyelectrolytes, the structure of the multilayer is influenced by pH[8,10,11] and ionic strength.[12,13] Further variables are the extent to which the two polyelectrolytes interpenetrate[14] and the extent of cross-linking and charge neutralization of one polymer by another. For multilayer growth, both linear and exponential growth regimes have been found.[15,16] In the latter case, the diffusion of one polyelectrolyte to the surface of the growing layer leads to an increase in layer thickness. At present, proposed applications of biopolyelectrolyte multilayers are largely in the biomedical area as encapsulation systems and coatings which can control cell adhesion,[7,9,17] although their functionality is relevant to other sectors including food. In this article, we wish to consider the interaction between two oppositely charged weak biopolyelectrolytes, pectin and poly-L-lysine. One motivation for examining the behavior of pectin is that fractions may be obtained in which varying proportions of the monomer units are charged such that the fractions differ in the average spacing between charges along the polymer backbone. Charge spacing can have a large effect on the swelling properties of polyelectrolyte networks.[18,19] At high charge densities, counterions can condense on the polymer backbone,[20] and at charge balance, collapsed structures are observed which have a minimal swelling.[21] For more weakly charged polyelectrolytes, this condensation is not observed, and the mobile counterions swell the network through a Donnan effect.[21−23]

The pectic polysaccharides are components of the primary cell wall and middle lamella of dicotyledonous plants. They are structurally complex and heterogeneous polyelectrolytes,[24,25] consisting of linear regions of (1→4)-α-D-galacturonosyl units and their methyl esters, interrupted in places by (1→2)-α-L-rhamnopyranosyl units. A fraction of these rhamnopyranosyl residues are branch points for neutral sugar side chains of (1→5)-α-L-arabinofuranosyl or (1→4)-β-D-galactopyranosyl residues. The average spacing between charges along the galacturonosyl backbone is inversely related to the methyl ester content. Pectins can form network structures with divalent counterions such as Ca^{2+} but also with basic biopolyelectrolytes such as chitosan and poly-L-lysine.[26,27] The affinity for the counterion increases with decreasing degree of esterification, DE. The DE of the pectin also has an effect on the swelling properties when it is cross-linked in a network. At neutral pH, in the presence of monovalent and divalent counterions, low DE pectin networks have a minimal swelling in water. With increasing DE, over the range 0−70%, there is an increased swelling.[21]

In this article, we examine the formation, by layer-by-layer assembly of pectin/poly-L-lysine multilayers. We have used surface plasmon resonance (SPR) to determine the mass of polymer deposited, Fourier transform infrared−attenuated total reflection spectroscopy (FTIR-ATR) to obtain information on the chemical characteristics of the deposited layers, and a quartz crystal microbalance with dissipation monitoring (QCMD) to obtain information on the hydration of the deposited layers.

* Corresponding author. Tel.: +44-1603-255000. Fax: +44-1603-507723. E-mail: steve.ring@bbsrc.ac.uk.

[†] Institute of Food Research.

[‡] University of Plovdiv "Paisii Hilendarski".

10.1021/bm0507249 CCC: $33.50
Published on Web 12/27/2005

Materials and Methods

Polyelectrolyte Solutions. Poly-L-lysine hydrobromide (PLL) with a mean degree of polymerization of 70 was obtained from Sigma; citrus pectins, from the same parent pectin and differing in degree of esterification, were obtained from CP Kelco; and citrus polygalacturonic acid was obtained from Fluka. D_2O (99.9%) was obtained from Sigma. Reagents were analytical grade. For multilayer fabrication, 0.6 mg mL^{-1} solutions of the polymers were prepared in 10 mM pH 7.0 phosphate buffer containing 30 mM NaCl.

Size Exclusion Chromatography. Chromatography of the pectins was carried out at room temperature on a polyhydroxymethacrylate gel packing using a Shodex SB-805 HQ column (0.8 × 30 cm) connected to a refractive index detector. The eluant was 0.2 M sodium acetate/0.1 M sodium nitrate at a flow rate of 0.4 mL min^{-1}. The injection volume was 50 μL of a 2.0 mg mL^{-1} polysaccharide solution. To establish the relationship between elution volume and molecular size, the column was calibrated with pullulan standards (Shodex, Showa Denko K. K.), of a limited polydispersity (M_w/M_n < 1.13). The standards were characterized by photon correlation spectroscopy to determine a hydrodynamic radius, R_h. The dependence of R_h on molecular weight was in agreement with published work.[28]

Surface Plasmon Resonance (SPR). Measurements were carried out using the Biacore X instrument (Biacore AB, Uppsala, Sweden). The sensing element was a thin film of gold (~50 nm) deposited on a glass substrate mounted in a sensor chip cartridge. The dimensions of the SPR cell were 50 × 500 × 2400 μm with a volume of 0.06 μL. The instrument monitors changes in refractive index adjacent to the surface of the gold film by measuring the intensity of polarized light reflected from the reverse side of the glass-gold interface. The plasmon resonance causes a minimum in intensity to occur at a certain angle of incidence, θ_m. The value of θ_m varies with changes in refractive index of the region adjacent to the gold surface. The size of this region depends on the penetration of an evanescent wave into the flow channel which typically extends 25−50% of the wavelength of the incident light from the surface.[29] The Biacore instrument reports θ_m in resonance units (RU) where 10 000 RU represents a shift in θ_m of 1°. The instrument was calibrated at 20 °C with methanol/water and sucrose/water mixtures of known refractive indices.[30] The response to changes in refractive index was found to be linear with a shift in θ_m of 86.6° per unit change in refractive index. The change in θ_m, $\Delta\theta$, due to the adsorption of a uniform adsorbed layer is related to refractive index through the relationship[29]

$$\Delta\theta = m(n_{adl} - n_s)[1 - \exp(-2h/d_{spr})] \quad (1)$$

where m is a calibration constant and n_{adl} and n_s are the refractive indices of the adsorbed layer and bulk solution, respectively. The thickness of the layer is h, and d_{spr} is the characteristic decay length of the evanescent electromagnetic field, which can be estimated as 37% ± 13% of the wavelength of incident light (760 nm).[29] If it is assumed that the refractive index of the adsorbed layer is proportional to the adsorbate concentration, the exponential in eq 1 can be expanded to yield an explicit equation for the mass of adsorbed polymer per unit area (c_{spr})

$$c_{spr} = \frac{d_{spr} c_{max} \Delta\theta}{2m(n_{ads} - n_s)} \quad (2)$$

where c_{max} and n_{ads} are the density and refractive index of the pure adsorbate. Expanding the exponential is accurate to within 10% when $h < 0.1\ d_{spr}$.

Multilayers were built up by the layer-by-layer technique. A buffer baseline was established, and then a PLL base layer was laid down by injecting 50 μL of PLL solution, followed by ~75 μL of buffer, 50 μL of pectin solution, and a buffer rinse as before. The sequence was repeated to form the multilayer. The gold surface was regenerated by flowing 0.1 M NaOH through the measurement cell. All measurements were made at 20 °C.

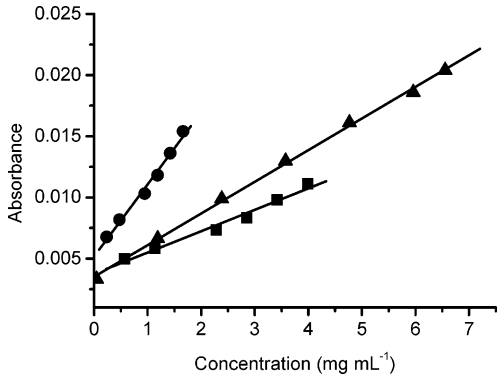

Figure 1. IR absorbance of PLL amide I (▲) (1645 cm^{-1}); galacturonate (●) (1610 cm^{-1}); uronic acid methyl ester (■) (1730 cm^{-1}), as a function of original solution concentration. The solution concentrations of galacturonate and its methyl ester were calculated from the known composition of the pectin (5A) used for calibration.

FTIR-ATR Spectroscopy. Infrared spectra were collected, over the range 4000−800 cm^{-1}, on a Nicolet 860 FTIR spectrometer (Thermo Electron Corporation, Madison USA) fitted with a MicroCircle liquid ATR cell (SpectraTech, Warrington, U.K.). The ATR crystal was a cylindrical ZnSe prism, with 11 internal reflections, mounted in a thermostated steel jacket set at a temperature of 20 °C. PLL and pectin solutions were prepared as described above using D_2O instead of H_2O. Multilayers were fabricated by the alternate deposition of PLL and pectin layers, with PLL forming the base layer. 1 mL of biopolymer solution was injected and left for 16 min. After each deposition step the cell was flushed with 2 mL of deuterated buffer. Spectra were accumulated by co-adding 1024 scans at a resolution of 2 cm^{-1} and referenced against a background of buffer alone.

In the ATR mode, a light beam strikes the interface between a medium of high refractive index (n_1) and a medium of low refractive index (n_2), the intensity of the beam is totally reflected if the angle of incidence θ_i is larger than the critical angle θ_c, where $\theta_c = \sin^{-1}(n_2/n_1)$. At the point of reflection, an evanescent wave of exponentially decreasing intensity penetrates the medium of lower refractive index. The penetration depth (d_{ir}) of the evanescent wave, defined as the distance normal to the interface at which the intensity falls to 1/e of the intensity at the surface, is given by

$$d_{ir} = \frac{\lambda}{2\pi n_1(\sin^2\theta_i - n_{12}^2)^{1/2}} \quad (3)$$

where λ is the wavelength of the light in a vacuum and $n_{12} = n_2/n_1$. The refractive index of the crystal is 2.41 and that of the dilute polymer in solution is 1.33. The angle of incidence is 45°. To quantify the FTIR response of the multilayer,[31−35] the penetration depth of the evanescent wave must be much larger than the thickness of the adsorbed layer. This is the case as the penetration depths for the relevant wavelengths range from 890 to 960 nm, whereas the maximum thickness of the layers was less than ~90 nm. Under this condition, it is assumed that the Beer−Lambert law applies. As the penetration depth is large compared to the layer thickness, the FTIR signal potentially contains contributions from the polymer in bulk solution as well as from the polymer adsorbed onto the surface of the crystal. However, at the concentrations used in the present experiment, the polymer in solution does not make a significant contribution to the observed spectra. Solution spectra of PLL and pectin were determined as a function of concentration over the concentration range 0−10 mg mL^{-1}. The peak heights of the characteristic absorbances of PLL[36] (1645 cm^{-1}) and pectin[37,38] (1610 and 1730 cm^{-1}) showed a linear dependence on concentration with a small positive intercept at zero concentration which was indicative of adsorbed material at the crystal surface (Figure 1).

If it is assumed that the amount of adsorbed material is independent of concentration in the range studied and that the amplitude of the

evanescent wave remains constant within the thin layer, then the mass per unit area (areal mass) of polymer adsorbed, c_{ir}, can be calculated from[31,39]

$$A = K\left(c_{ir} + \frac{c_s d_{ir}}{2}\right) \quad (4)$$

where A is the peak absorbance for nonpolarized light, K is a constant, and c_s is the bulk solution concentration. The penetration depth, d_{ir}, calculated from eq 3, ranges from ~958 nm at 1610 cm^{-1} (carboxylate); ~938 nm at 1645 cm^{-1} (amide I); and ~892 nm at 1730 cm^{-1} (ester). The values of K obtained were 1.27×10^{-4} (carboxylate); 5.52×10^{-5} (amide I) and 3.93×10^{-5} ng cm^{-2} (ester). This calculation allows the mass of PLL and pectin deposited during the formation of the multilayer to be determined, together with the ester content of the deposited pectin layer.[38]

Quartz Crystal Microbalance. Measurements were carried out using a D300 quartz crystal microbalance with dissipation monitoring (QCMD) (Q-Sense AB, Västra Frölunda, Sweden) with a QAFC 302 axial flow measurement chamber. The sensing element is a disc-shaped, AT-cut piezoelectric quartz crystal sandwiched between two gold electrodes. An AT-cut crystal is one that is cut at 35° to the y axis of the quartz crystal. The crystal is excited to oscillation at its fundamental resonant frequency (~5 MHz). A small mass deposited (Δm) on the gold sensing surface will cause a decrease in resonant frequency (Δf). If the mass is deposited evenly and is sufficiently rigid then the mass adsorbed is directly proportional to the change in frequency according to the Sauerbrey equation[40]

$$\Delta m = -C\Delta f/n \quad (5)$$

where C is the mass sensitivity constant ($C = 17.7$ ng cm^{-2} Hz^{-1} for a 5 MHz crystal[41]) and n is the overtone number ($n = 1, 3, 5, ...$). For elastic, cross-linked gel networks, the mass of solvent trapped within the gel contributes to the overall mass adsorbed and the observed frequency change. For viscoelastic materials, the adsorbed mass does not fully couple to the oscillation of the crystal and hence dampens the oscillation. The QCMD measures this dissipation from the response of the crystal at its resonant frequency (5 MHz) and at three of its overtones (15, 25, or 35 MHz) following the excitation of the crystal to resonance. The decrease in the amplitude of the oscillation with time provides a single-exponential decay constant which characterizes the dissipation.

The QCMD response to dissipative viscoelastic films has been modeled using a Voigt model.[42] The full expression for the resonance frequency and dissipation shifts with thick adsorbed layers can be concisely expressed using complex variables.[42] Some physical insight into how the material properties of the bulk liquid and adsorbed layer affect the QCMD response can be obtained for single thin viscoelastic adsorbed layers for which the equations simplify as follows (retaining Voinova et al.'s[42] notation)

$$\Delta f \approx -\frac{1}{2\pi\rho_0 h_0}\left\{\frac{\eta_3}{\delta_3} + h_1\rho_1\omega - 2h_1\left(\frac{\eta_3}{\delta_3}\right)^2 \frac{\eta_1\omega^2}{\mu_1^{\,2} + \omega^2\eta_1^{\,2}}\right\} \quad (6)$$

$$\Delta D \approx \frac{1}{\pi f\rho_0 h_0}\left\{\frac{\eta_3}{\delta_3} + 2h_1\left(\frac{\eta_3}{\delta_3}\right)^2 \frac{\mu_1\omega}{\mu_1^{\,2} + \omega^2\eta_1^{\,2}}\right\} \quad (7)$$

where ρ_0 and h_0 are the density and thickness of the crystal, respectively. The viscosity of the bulk liquid is η_3, and δ_3 ($=(2\eta_3/\rho_3\omega)^{1/2}$) is the viscous penetration depth of the shear wave in the bulk liquid and ρ_3 is the liquid's density. The thickness, density, viscosity and elastic shear modulus of the adsorbed layer are represented by h_1, ρ_1, η_1, and μ_1, respectively; ω is the angular frequency of the oscillation. The first term in the brackets in eqs 6 and 7, η_3/δ_3, is the frequency and dissipation shift due to immersing the crystal oscillator in the bulk liquid, a term which is effectively constant in our experiments. The second term in the brackets in eq 6 is the Sauerbrey term, as in eq 5, due to the hydrated mass of the adsorbed layer. As this term is proportional to frequency, it is common to present the frequency shift as $\Delta f/n$ to take this into account. The final term in the brackets in eq 6 and 7 arises due to the viscoelasticity of the adsorbed layer. In eq 6 this term is negative so that viscoelasticity reduces the frequency shift and the use of the Sauerbrey equation would underestimate the mass adsorbed and hydrated layer thickness. Modeling software (QTools) supplied with the QCMD uses the full thick layer expressions to model the response. The program finds a best fit using a Simplex algorithm to find the minimum in the sum of the squares of the scaled errors between the experimental and model Δf and ΔD values. By assuming the density and viscosity of the bulk liquid (ρ_3 and η_3) are 1000 kg m^{-3} and 1.0 mPa s, respectively, and a fixed density of the layer (ρ_1), the package estimates the viscosity, shear modulus and the thickness of the adsorbed layer.

Table 1. Pectin Characteristics: Anhydrogalacturonic Acid Content (GalA), Average Degree of Esterification, and Hydrodynamic Radius (R_h)

pectin identity code	% w/w GalA	% DE	R_h (nm)
5A	85	71	10.2
5C	91	51	10.0
5E	92	36	7.1
5G	94	21	10.6
PGA	90	0	7.1

The formation of multilayers was investigated at 20 °C using the same biopolymer solutions as described above. Starting with the system primed with buffer solution, a base layer is formed by first flowing ~1.5 mL of PLL solution into a thermostatic coil in the measurement head to flush out the previous solution and allow the solution to reach thermal equilibrium. After 2 min, ~0.5 mL of this solution was allowed to flow into the measurement cell to replace the existing solution, driven by the head of liquid in the sample reservoir which flows into the thermostatic coil. The same procedure was repeated with buffer, followed by pectin solution, buffer solution, and so on, until 10 biopolymer layers were deposited. Between each experiment, the crystal chip was cleaned by sonication in 99% ethanol solution for 5 min followed by sonication in 2% Hellmanex solution for 5 min. The chips were rinsed in distilled water and then dried with N_2.

Results and Discussion

Pectin Characterization. The neutral sugar composition and a fragmentation analysis of the distribution of free galacturonosyl residues along the polymer backbone was previously described for pectins 5E and 5G,[26,43] and pectins 5A and 5C were characterized in the same way (unpublished). The galacturonic acid content was in the range 85−94% (Table 1) with the balance of the residues consisting of the neutral sugars arabinose and galactose.

The average degree of esterification of the galacturonosyl residues ranged from 0 to 71%. The distribution of free galacturonosyl residues was essentially random as confirmed by the chemical fragmentation analysis.[26] The pectins were subjected to size exclusion chromatography, and all gave rather broad peaks with peak maxima in refractive index response corresponding to hydrodynamic radii (R_h) in the range 7.1−10.6 nm. For all pectins, the elution profiles were asymmetrical and skewed to the larger molecular sizes with small amounts of material (5−10%) eluting in the size range of 23−37 nm. Comparison with literature pectin characterizations[44] indicate that these pectins have smaller than average R_h suggesting a limited degradation and/or fractionation during their preparation. At pH 7.0, the PLL can be represented as an equivalent random

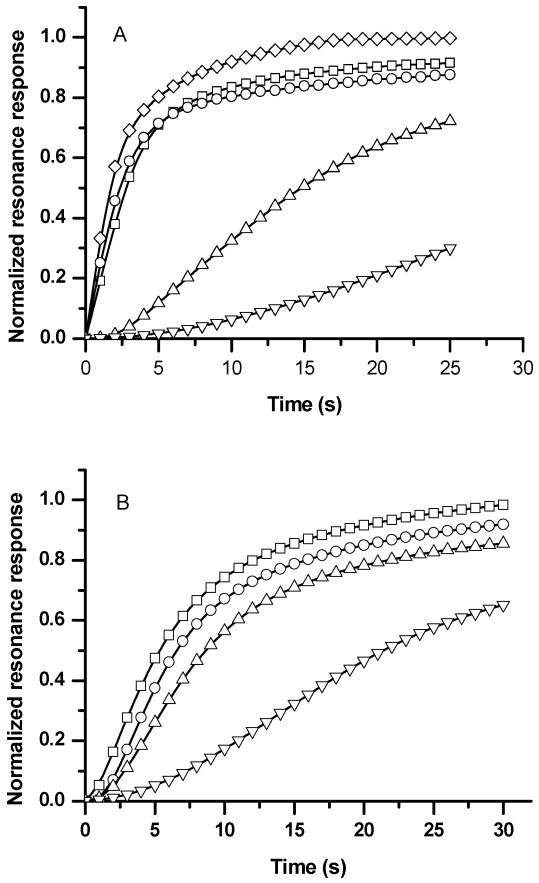

Figure 2. SPR measurement of pectin (A) and PLL (B) adsorption kinetics as a function of flow rate (μL min^{-1}): 1 (▽); 5 (△); 25 (○); 50 (□); and 100 (◇).

coil with an R_h estimated from its DP of about 2.6 nm[45] and so the pectin R_h are a factor of 2.7−4.0 larger than the PLL.

Surface Plasmon Resonance. Multilayers are nonequilibrium structures, and it is important to consider how the conditions of their formation influence their characteristics. In previous research,[46] we have found that the mass of polymer deposited increased with increasing solution concentration of polymer, which is the generally observed behavior for the nonequilibrium adsorption of polymers at surfaces.[47] At low concentrations, the polymer binds and then spreads out on the surface, whereas at higher concentrations, the spreading is inhibited by neighboring polymer molecules.[47] A further consideration is how the transport of polyelectrolyte to the multilayer surface influences behavior.[48,49] Preliminary experiments examined the effect of sample flow rate on association of the biopolymer to the surface of the growing multilayer. In Figure 2A is shown the effect of flow rate through the measurement cell on the binding of pectin (5E) to an initial PLL layer for flow rates in the range 1.0−100.0 μL min^{-1}. The resonance response was normalized relative to the limiting plateau of response at longer times. The normalized response showed a marked dependence on flow rate in the range 1.0−5.0 μL min^{-1} but became essentially independent of flow at a rate of >25.0 μL min^{-1}. For the binding of PLL to the pectin layer (Figure 2B), a similar trend was observed although the effect at the lower flow rates was less marked and is probably related to the smaller molecular size and faster diffusion of PLL compared to pectin. The remainder of the experiments were conducted at a flow rate of 25.0 μL min^{-1}.

In Figure 3A−E is shown the calculated mass adsorbed per unit area for pectin/PLL multilayers formed from pectins differing in their average degree of esterification from 0 to 71%. The inset in each figure shows the SPR response for the deposition of the 5th (PLL) and 6th (pectin) layers. For each pectin and PLL layer, there is a progressive increase in mass deposited with an increase in layer number. This type of behavior is observed for multilayers in which one of the components can diffuse to the growing multilayer surface.[50,51] For all of the pectins examined, the form of the growth of the multilayer is similar, as is the total mass of the multilayer deposited. The insets (Figure 3A−E) on the growth of the 5th and 6th layers show comparable behavior for all of the pectins examined. There is a marked increase in resonance response which rapidly reaches a plateau for the deposition of PLL on a pectin layer. A small decrease in response rapidly reaches a plateau on flowing over buffer, which can be attributed to a limited solubilization of PLL, followed by a further marked increase in response as the pectin layer is deposited. Flowing buffer over the pectin layer results in a limited solubilization of pectin which is somewhat more marked for the layer formed from pectin having the highest average DE (71% DE, pectin 5A, Figure 3A). For each layer pair, the mass of PLL deposited is somewhat larger than the mass of pectin deposited, with the pectin/PLL ratio ranging from 0.83 to 0.97 (Table 2). The affinity of cationic polyelectrolytes for pectin is dependent on the average charge spacing between the carboxylate groups along the pectin chain, with the affinity for the polycation increasing with decreasing DE.[26,27] The results obtained on the growth of pectin/PLL multilayers suggest that, over the range of average DEs studied, the affinity between PLL and pectin does not have a large influence on growth. A further consequence of the similar patterns of growth for the different pectin multilayers is that the polyanion/polycation charge balance in the multilayers is expected to be very different. As pectin preparations will contain a population of molecules differing in DE, it is important to establish whether the deposition of pectin involves any fractionation of this population. We have used FTIR-ATR to probe the chemical characteristics of the deposited species.

FTIR-ATR. Figure 4A shows the FTIR spectra of pectin 5A and PLL. As the intrinsic pK of the uronic acid of pectin is 3−3.5,[52] at pHs in the vicinity of neutrality, the uronic acid will be fully charged and can be recognized in the FTIR spectrum from the strong absorbance from the asymmetric stretching of COO^- at ∼1607−1617 cm^{-1}. The absorbance of the C═O stretching vibration of the uronic acid methyl ester[38] occurs at ∼1730 cm^{-1}, and the amide I band of poly-L-lysine in a random coil conformation[36] has a strong absorbance in the range 1643−1648 cm^{-1}. The assembled multilayers had absorbances characteristic of these functional groups. Figure 4B−F shows the FTIR spectra in the range 1540−1775 cm^{-1} for the fabrication of pectin/PLL multilayers at pH 7 for pectins differing in DE, i.e., 5A (71%), 5C (51%), 5E (36%), 5G (21%), and PGA (0%), respectively. Deposition of each layer resulted in characteristic spectral changes, an increase in the absorbance of the amide I band when PLL was deposited, and an increase in carboxylate and ester bands when pectin was deposited. From these data, it is possible to calculate multilayer growth curves for the pectin/PLL layers. The form of the growth of the multilayer (Figure 5A−E) are in good agreement with those obtained by SPR, with the exception of the multilayer formed from the most highly esterified pectin. In the FTIR spectra (Figure 4B), the top two layer pairs show a reduction in absorbance in the amide peak when the pectin is added. This loss in absorbance indicates that, under the conditions of the

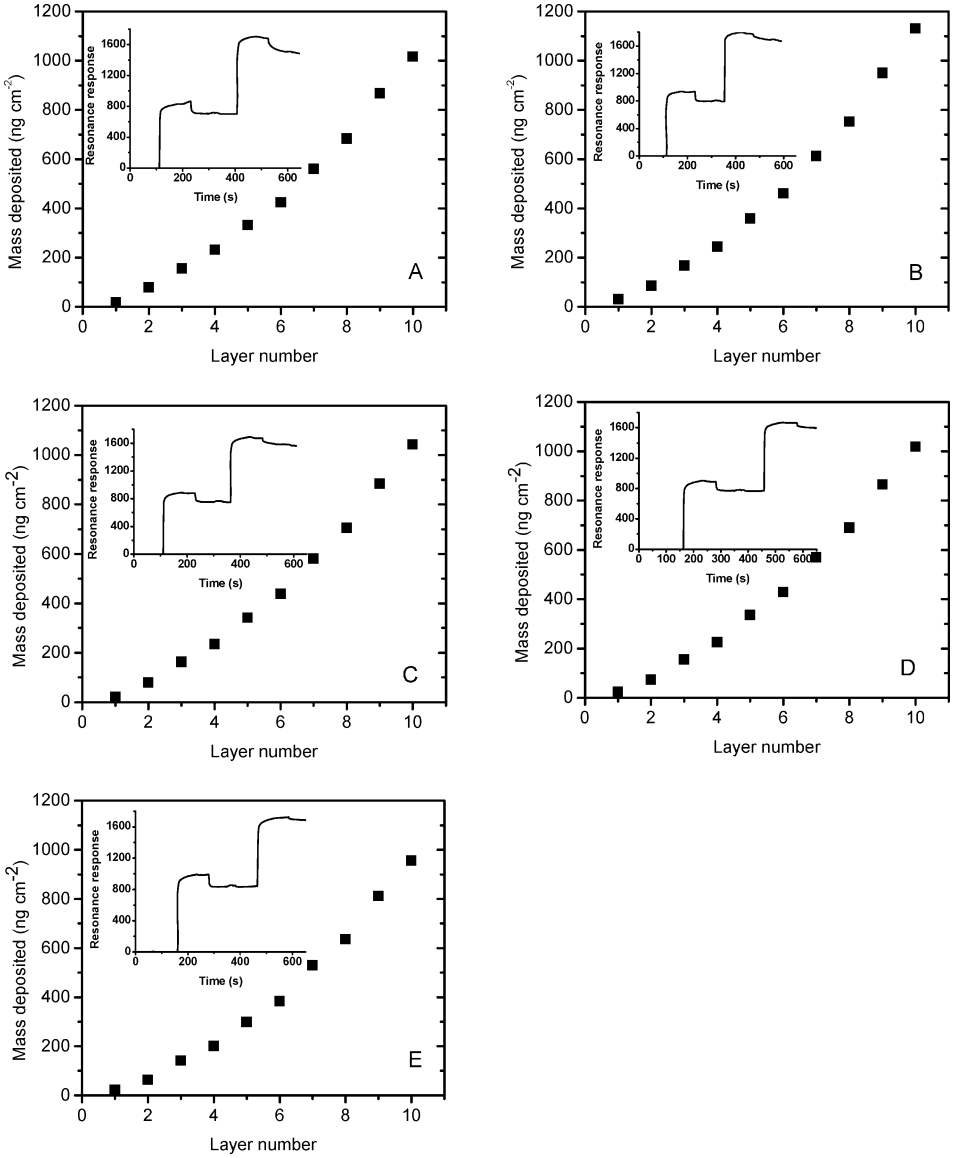

Figure 3. Plot of mass of polymer deposited after buffer wash, obtained from SPR response, versus layer number for the deposition of a pectin/PLL multilayer (starting with PLL) for pectin 5A (A); 5C (B); 5E (C); 5G (D); and PGA (E). Inset shows the resonance response as a function of time for the deposition of the 5th and 6th layers.

Table 2. Pectin/PLL Multilayer Characteristics: Degree of Esterification of Pectin Deposited, Pectin/PLL Ratio, and Polyanion/Polycation Charge Ratio from FTIR-ATR and SPR Data

pectin identity code	initial % DE	deposited % DE	pectin/PLL SPR	charge ratio SPR
5A	71	55	0.97	0.32
5C	51	38	0.95	0.42
5E	36	25	0.96	0.52
5G	21	18	0.91	0.54
PGA	0	0	0.83	0.60

FTIR experiment, some stripping of the PLL from the multilayer by the pectin in solution occurs. This removal of PLL means that there is less PLL present to capture the next pectin layer. This small loss of PLL is coincident with pectin deposition and would not be observed in the SPR response which is sensitive to a net change in mass.

The estimates of the amount of material deposited differ between the techniques and might reflect the differences in surface chemistry or roughness of the initial surface in these measurement systems. From the FTIR spectra, it is possible to estimate the DE of the pectins which were deposited (Table 2). For each pectin the material deposited had a lower DE than the average DE of the pectin sample. Determination of the DE of the deposited pectin allows calculation of the polyanion/polycation charge balance within the layers. This calculation was performed on the SPR data, assuming that the subfractionation of the pectin population was similar in the FTIR and SPR experiments. In all cases, the polyanion/polycation charge ratio was less than unity, progressively decreasing from 0.60 to 0.32 as the DE is increased from 0 to 71% (Table 2).

QCMD. The QCMD measurements complement those of the SPR and FTIR-ATR as the technique is sensitive to the hydrated mass of the adsorbed multilayer. Figures 6, panels A and B, and 7, panels A and B, show the successive frequency and dissipation shifts for the deposition of 10 layer multilayers, consisting of alternating PLL and pectin layers, for pectin 5A (71% DE) and pectin 5G (21% DE), respectively. Each layer addition was separated by a buffer wash. A characteristic of the pectin/PLL multilayer build-up is the shrinkage on addition of the PLL indicated by the reduction in $-\Delta f/n$ which is

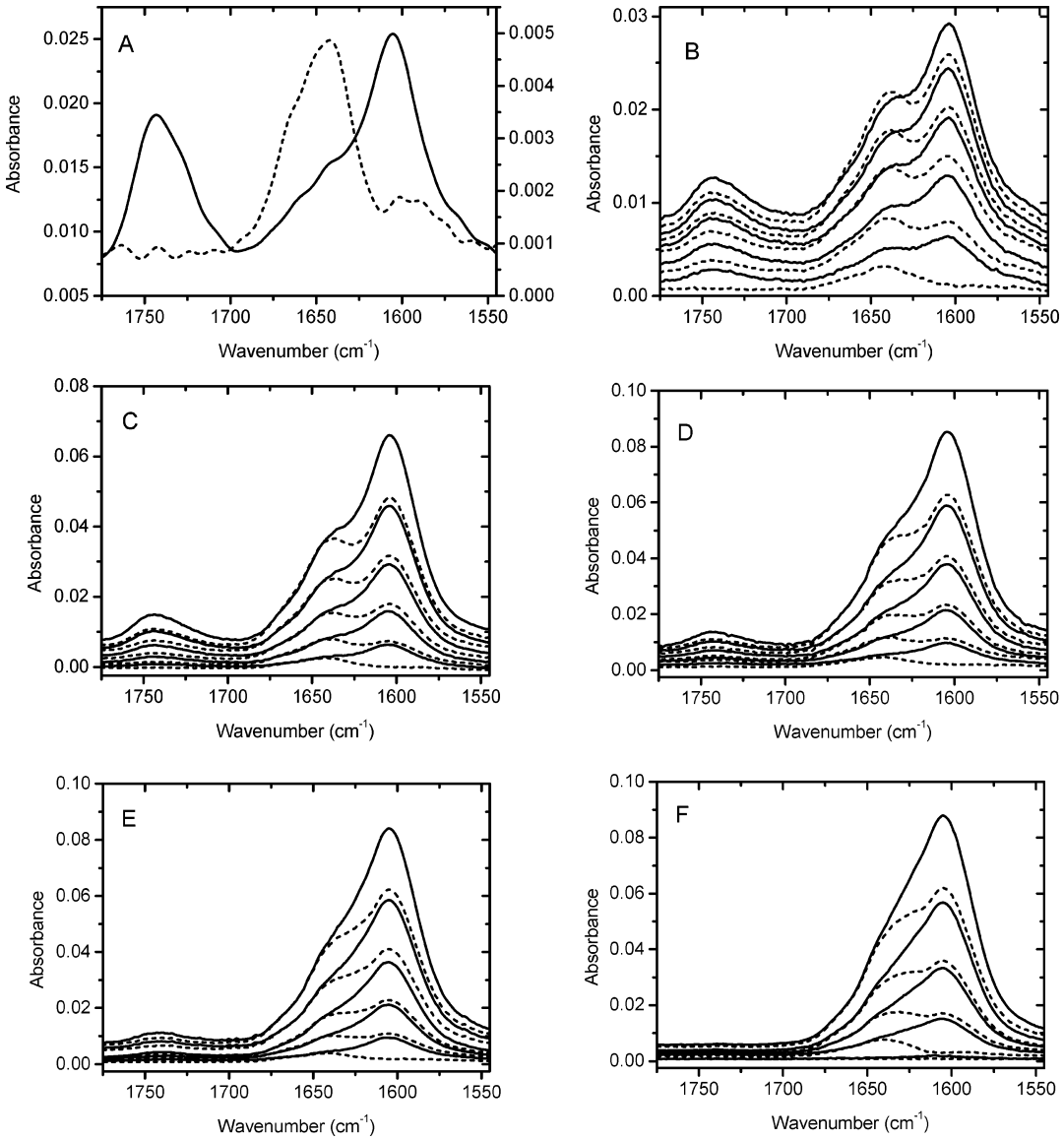

Figure 4. FTIR spectra of pectin 5A in D_2O at 10 mg mL^{-1} (solid line, left axis) and PLL at 3 mg mL^{-1} (dashed line, right axis) (A) and for the successive deposition of a pectin (solid line) /PLL (dashed line) multilayer for pectin 5A (B); 5C (C); 5E (D); 5G (E); and PGA (F).

particularly strong in pectin 5A (Figure 6A). The finite dissipation (Figures 6B and 7B) indicates that the multilayers are viscoelastic rather than rigid elastic and so it is appropriate to analyze the data using the Voigt-model of Voinova et al.[42] rather than the simpler Sauerbrey expression (eq 5). In Voinova's thin-layer expression for the frequency shift (eq 6), the Sauerbrey term, $h_1\rho_1\omega$, contains the product of layer thickness (h_1) and density (ρ_1) which means these quantities cannot readily be independently extracted from the QCMD measurements. In our analysis a layer density of 1100 kg m^{-3} is assumed, and from this, a hydrated areal mass ($h_1\rho_1$) is calculated. The areal mass was found to be independent of the assumed layer density within the range 1000−1200 kg m^{-3}.

Table 3 summarizes the overall mean thicknesses (average of 3−4 runs) for buffer washed multilayers obtained from the QCMD experimental data using QTools and estimates of the solids concentrations which were calculated by combining the areal masses from the SPR with those from the QCMD experiment. In both techniques, the initial deposition was PLL to a gold surface and the estimates are dependent on there being a similar multilayer deposition in the two experiments. Calculations are presented for multilayers with 8−10 layers which reveal the essential characteristics of the build up of successive layers. First we consider the multilayers where pectin is the uppermost layer (8 and 10 layers). The lowest charge density pectins (5A and 5C) form the thickest, most highly hydrated multilayers with a solids concentration in the range 10−13% w/w. Thinner, denser multilayers, with a solids concentration in the range 19−32% w/w, are formed from the higher charge density pectins (5E and 5G) and polygalacturonic acid. Comparing the increase in multilayer thickness on addition of the final pectin layer with the hydrodynamic diameter of the pectin (Table 1) indicates that, for the lowest charge density pectins (5A and 5C), the multilayer is growing by 33−39 nm compared with a hydrodynamic diameter of 20 nm. One explanation for this behavior is that the larger pectin species are preferentially deposited from the polydisperse pectin preparation, and alternatively it indicates that the PLL can diffuse into the freshly deposited pectin layer and can "capture" further pectin molecules. The diffusion of PLL in multilayers has already been suggested as the origin of exponential-type growth in these types of structure.[53,54] If the PLL is mobile within the multilayer, this means that any layering of the two macromolecules created by the sequential deposition will diminish with time leading to a

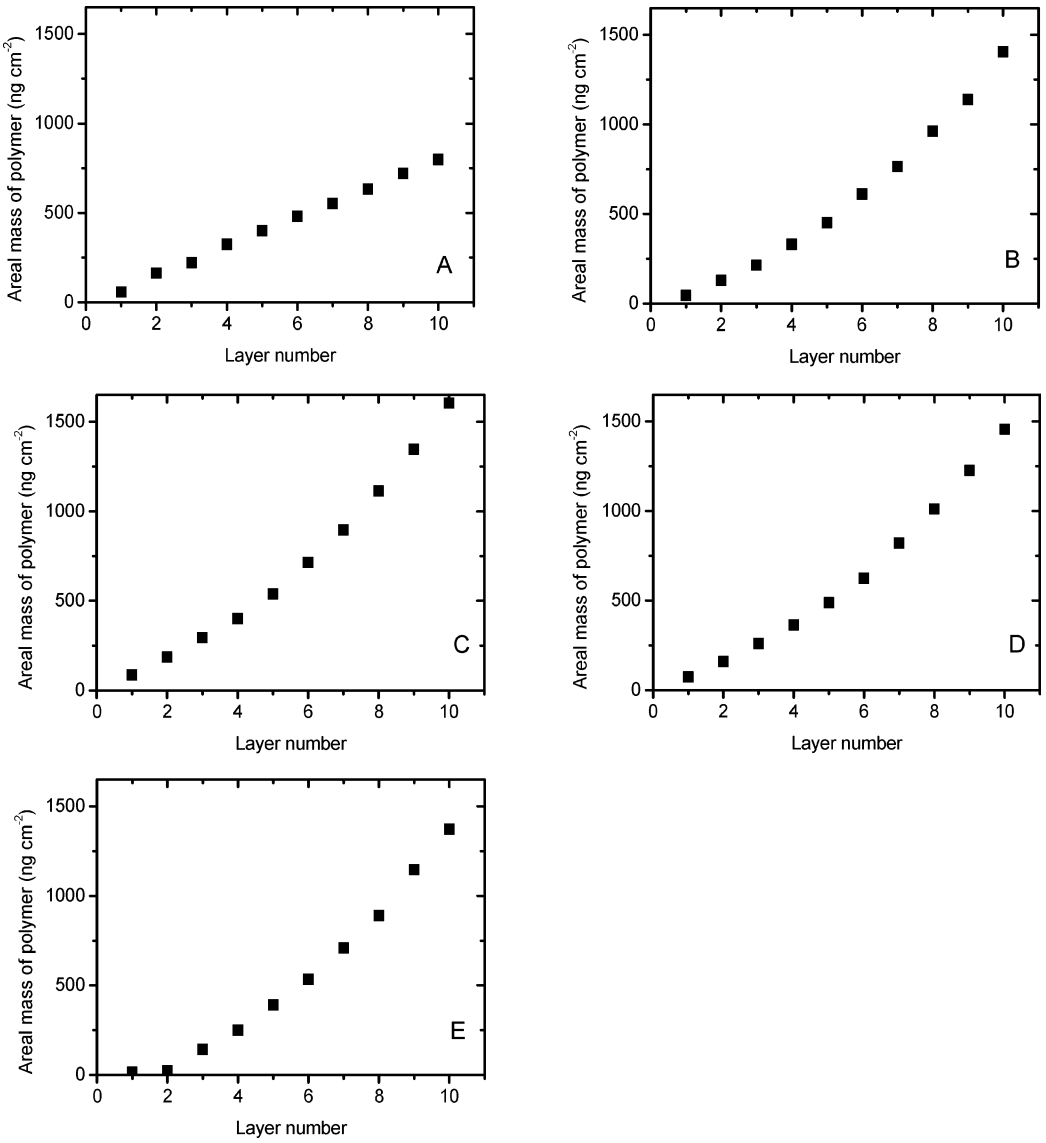

Figure 5. Plot of mass of polymer deposited after buffer wash, calculated from FTIR absorbance, versus layer number for the deposition of a pectin/PLL multilayer for pectin 5A (A); 5C (B); 5E (C); 5G (D); and PGA (E).

more homogeneous structure. In this context, the term "multilayer" refers only to how the structure was fabricated and may not be an appropriate description of the aged structure.

The other feature which is revealed in the QCMD experiment on the buildup of pectin/PLL multilayers is the collapse in multilayer thickness which is observed on addition of PLL. In experiments on the swelling of pectin/PLL gels, it was found that, at a fixed osmotic stress, addition of PLL up to charge balance, progressively suppressed the swelling of the gel.[26] A more highly cross-linked structure is more resistant to swelling. In addition, through balancing the charge on the network with a polycationic counterion rather than a monovalent counterion, the magnitude of the osmotic pressure of the network generated through a polyelectrolyte effect is also expected to be reduced.[22] The magnitude of the collapse induced by addition of PLL is quantified by the thickness ratio for the multilayers consisting of 8 and 9 layers (Table 3). The effect is most marked for the lowest charge density pectin (5A); it no longer occurs for the polygalacturonic acid, and the overall trend is a decrease with increasing charge density. This is consistent with observations on the swelling of pectin films as a function of DE and osmotic stress.[21] It was found that, whereas the more highly charged pectins and polygalacturonic acid formed collapsed structures, with decreasing charge density there was, at a fixed osmotic stress, an increased swelling. These observations are also consistent with the known general behavior of the dependence of the swelling of polyelectrolytes on average charge spacing along the polymer chain.[19] The mobile counterions of a weakly charged polyelectrolyte network generate a swelling pressure through a Donnan effect, whereas at high charge densities, counterion condensation provokes network collapse.

The buffer washing results in a time dependent reduction in the negative frequency and dissipation shifts (Figures 6 and 7). This effect is most marked when washing a pectin layer. Some of the change in dissipation response is instantaneous. Analysis with QTools indicates this is due to a step decrease in thickness (h_1) and step increase in viscosity (η_1). This suggests that an outer, weakly adsorbed layer is removed during the buffer washing leaving a relatively viscous sublayer.

Modeling the experimental data using the Voigt model provides both a viscoelastic correction to the Sauerbrey estimates of the areal mass and also viscoelastic parameters characterizing the rheological properties of the multilayer. The magnitude of the viscoelastic thick layer correction is typically 40−60% for our multilayers; that is, the thickness estimated using the Voigt model is on average 40−60% greater than the thickness

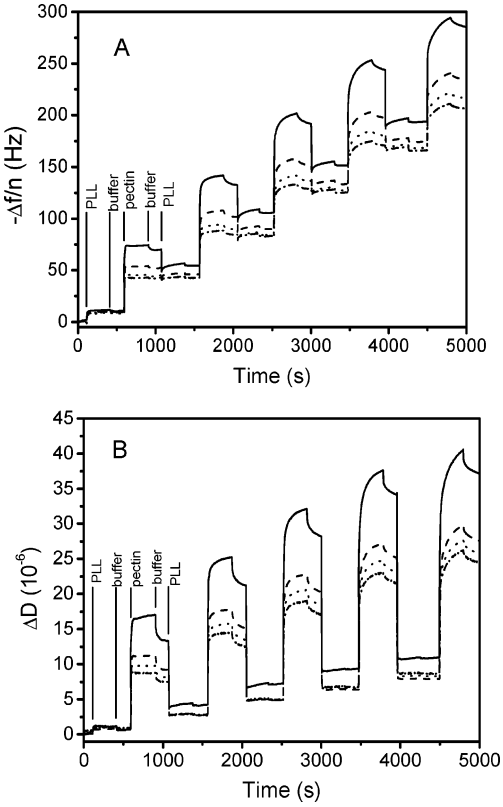

Figure 6. QCMD frequency (A) and dissipation (B) shifts during the build up of pectin 5A (71% DE)/PLL multilayers. Frequencies: solid line, 5 MHz; dashed line, 15 MHz; dotted line, 25 MHz; dot−dashed line, 35 MHz.

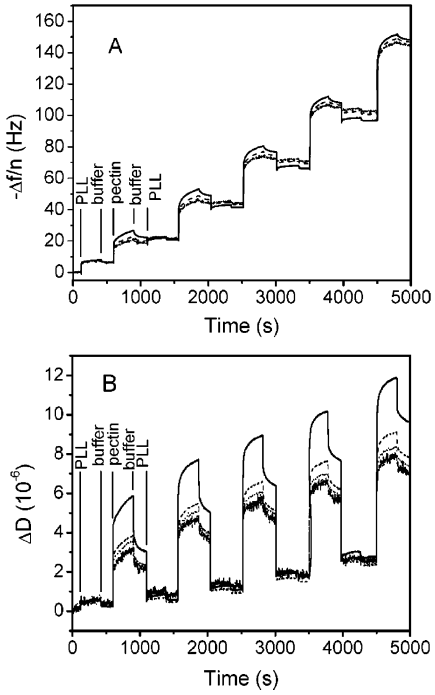

Figure 7. QCMD frequency (A) and dissipation (B) shifts during the build up of pectin 5G (21% DE)/PLL multilayers. Frequencies: solid line, 5 MHz; dashed line, 15 MHz; dotted line, 25 MHz; dot−dashed line, 35 MHz.

estimated using the Sauerbrey equation from the frequency shift of the 15 MHz overtone which is commonly accepted to be the single most accurate measurement. In comparison to the estimates of the multilayer thickness, the estimates of rheological properties are more variable. In Figures 6B and 7B, the dissipation has a weak dependence upon frequency which for these multilayers is associated with predominantly viscous behavior with the viscoelastic ratio ($\mu_1/\omega\eta_1$), evaluated at the mid frequency (20 MHz), being about 0.1 for 8−10 layer multilayers. For both these pectins on collapse of the 8-layer multilayer to the 9-layer multilayer, the mean viscosity increases from 2.5 to 4.0 mPa s before reducing to 3.2 mPa s for the 10-layer multilayer, a variation consistent with the variation of solids content. On the collapse there is a corresponding increase in shear modulus by a factor of 1.6 thus maintaining the constancy of the viscoelastic factor.

General Discussion. PLL can be an effective low molecular weight cationic cross-linker of pectin gels. This gelation is sensitive to the DE of the pectins. Increasing DE above ~40%, reduces gelation, whereas decreasing DE results in the formation of collapsed structures. Pectin/PLL multilayer formation shows similar trends, the higher DE pectins form more open, hydrated structures, with more compact structures forming as the DE is reduced. In the formation of the multilayer, there is a limited fractionation of pectin, with the DE of the deposited pectin being lower than the average DE of the pectin fraction. Even so, the pectin layers in the multilayers prepared from the different pectin fractions have characteristically different DEs. The build up in mass of the multilayer shows that a slight excess of PLL is deposited even though the pectin has the larger macromolecular size. This suggests that the lower molecular weight PLL has the ability to diffuse into and cross-link the pectin layer. The multilayer structure could be viewed as a succession of pectin/PLL gel layers with sufficient overcharging of the pectin layers to permit the subsequent deposition of another pectin layer. It has been suggested that it is this ability of PLL to diffuse within the polysaccharide layer that is the origin of the observed exponential growth of the multilayer in this type of system.[54] The observations of the current study, particularly from the QCMD data, support this suggestion. Even for the PGA/PLL networks, the polyanion/polycation charge ratio is less than unity with an excess of positive charge within the network. This suggests that the interaction between PGA and PLL does not lead to the formation of a 1:1 complex under these conditions.

Table 3. Mean Multilayer Thicknesses (after Buffer Rinsing), Solids Concentrations, and Thickness Ratios for Final Three Layers Added to Pectin/PLL Multilayers[a]

pectin identity code	h_1, 8 layers (nm)	h_1, 9 layers (nm)	h_1, 10 layers (nm)	solids conc., 8 layers (% w/w)	solids conc., 9 layers (% w/w)	solids conc., 10 layers (% w/w)	thickness ratio, 9 layers/8 layers	thickness ratio, 10 layers/9 layers
5A	67	42	75	10	19	13	0.63	1.79
5C	70	49	88	10	18	12	0.70	1.80
5E	36	33	48	19	27	21	0.92	1.45
5G	31	23	37	21	32	24	0.74	1.60
PGA	32	33	42	19	24	22	1.03	1.27

[a] Multilayer thicknesses calculated assuming density of 1100 kg m^{-3}.

For short linear chains of PGA and PLL the average spacing between charges is 0.44 and 0.38 nm,[45] respectively. The progressive esterification of the anhydrogalacturonosyl residues of the pectin chain increases the average spacing between charges and leads to the formation of pectin/PLL layers with an increasing excess of positive charge.

Conclusions

Pectin/PLL multilayers were fabricated from a range of pectin fractions differing in the average spacing between charges. The form of the growth of the multilayer was consistent with the proposal that low molecular weight PLL is able to diffuse through the multilayer to the growing surface resulting in a progressive increase in mass of material deposited with each deposition. The net charge of the multilayers was positive. Although some subfractionation of the pectin fractions occurred during multilayer fabrication, the nonequilibrium nature of the fabrication resulted in the formation of multilayers with a range of charge ratios.

Acknowledgment. The UK Biotechnology and Biological Sciences Research Council supported this research from the core strategic grant and through the award of a studentship to J.M. (BBSSK200310164). M.M. acknowledges support from an EC Marie Curie fellowship (Contract Number QLK-1999-50512). A.K. acknowledges support from an EC Leonardo fellowship.

References and Notes

(1) Mattison, K. W.; Dubin, P. L.; Brittain, I. J. *J. Phys. Chem. B* **1998**, *102*, 3830−3836.
(2) Zintchenko, A.; Rother, G.; Dautzenberg, H. *Langmuir* **2003**, *19*, 2507−2513.
(3) Weinbreck, F.; de Vries, R.; Schrooyen, P.; de Kruif, C. G. *Biomacromolecules* **2003**, *4*, 293−303.
(4) Decher, G. *Science* **1997**, *277*, 1232−1237.
(5) Quinn, J. F.; Caruso, F. *Langmuir* **2004**, *20*, 20−22.
(6) Lavalle, P.; Vivet, V.; Jessel, N.; Decher, G.; Voegel, J. C.; Mesini, P. J.; Schaaf, P. *Macromolecules* **2004**, *37*, 1159−1162.
(7) Elbert, D. L.; Herbert, C. B.; Hubbell, J. A. *Langmuir* **1999**, *15*, 5355−5362.
(8) Burke, S. E.; Barrett, C. J. *Biomacromolecules* **2003**, *4*, 1773−1783.
(9) Richert, L.; Lavalle, P.; Payan, E.; Shu, X. Z.; Prestwich, G. D.; Stoltz, J. F.; Schaaf, P.; Voegel, J. C.; Picart, C. *Langmuir* **2004**, *20*, 448−458.
(10) Shiratori, S. S.; Rubner, M. F. *Macromolecules* **2000**, *33*, 4213−4219.
(11) Kato, N.; Schuetz, P.; Fery, A.; Caruso, F. *Macromolecules* **2002**, *35*, 9780−9787.
(12) Kovacevic, D.; van der Burgh, S.; de Keizer, A.; Stuart, M. A. C. *Langmuir* **2002**, *18*, 5607−5612.
(13) Dubas, S. T.; Schlenoff, J. B. *Macromolecules* **2001**, *34*, 3736−3740.
(14) Schlenoff, J. B.; Dubas, S. T. *Macromolecules* **2001**, *34*, 592−598.
(15) Hubsch, E.; Ball, V.; Senger, B.; Decher, G.; Voegel, J. C.; Schaaf, P. *Langmuir* **2004**, *20*, 1980−1985.
(16) Lavalle, P.; Gergely, C.; Cuisinier, F. J. G.; Decher, G.; Schaaf, P.; Voegel, J. C.; Picart, C. *Macromolecules* **2002**, *35*, 4458−4465.
(17) Richert, L.; Lavalle, P.; Vautier, D.; Senger, B.; Stoltz, J. F.; Schaaf, P.; Voegel, J. C.; Picart, C. *Biomacromolecules* **2002**, *3*, 1170−1178.
(18) Rubinstein, M.; Colby, R. H.; Dobrynin, A. V.; Joanny, J.-F. *Macromolecules* **1996**, *29*, 398−406.
(19) Kokufuta, E.; Wang, B. L.; Yoshida, R.; Khokhlov, A. R.; Hirata, M. *Macromolecules* **1998**, *31*, 6878−6884.
(20) Manning, G. S.; Ray, J. *J. Biomol. Struct. Dyn.* **1998**, *16*, 461−476.
(21) Ryden, P.; MacDougall, A. J.; Tibbits, C. W.; Ring, S. G. *Biopolymers* **2000**, *54*, 398−405.
(22) Flory, P. J. *Principles of Polymer Chemistry*; Cornell University Press: Ithica, NY, 1953.
(23) MacDougall, A. J.; Rigby, N. M.; Ryden, P.; Tibbits, C. W.; Ring, S. G. *Biomacromolecules* **2001**, *2*, 450−455.
(24) Schols, H. A.; Posthumus, M. A.; Voragen, A. G. J. *Carbohydr. Res.* **1990**, *206*, 117−129.
(25) Schols, H. A.; Voragen, A. G. J. *Carbohydr. Res.* **1994**, *256*, 83−95.
(26) Marudova, M.; MacDougall, A. J.; Ring, S. G. *Carbohydr. Res.* **2004**, *339*, 209−216.
(27) Marudova, M.; MacDougall, A. J.; Ring, S. G. *Carbohydr. Res.* **2004**, *339*, 1933−1939.
(28) Nishinari, K.; Kohyama, K.; Williams, P. A.; Phillips, G. O.; Burchard, W.; Ogino, K. *Macromolecules* **1991**, *24*, 5590−5593.
(29) Jung, L. S.; Campbell, C. T.; Chinowsky, T. M.; Mar, M. N.; Yee, S. S. *Langmuir* **1998**, *14*, 5636−5648.
(30) *Handbook of Chemistry and Physics*, 55th ed.; CRC Press: Boca Raton, FL, 1974.
(31) Sperline, R. P.; Muralidharan, S.; Freiser, H. *Langmuir* **1987**, *3*, 198−202.
(32) Sukhishvili, S. A.; Dhinojwala, A.; Granick, S. *Langmuir* **1999**, *15*, 8474−8482.
(33) Sukhishvili, S. A.; Granick, S. *J. Chem. Phys.* **1999**, *110*, 10153−10161.
(34) Sukhishvili, S. A.; Granick, S. *J. Chem. Phys.* **1998**, *109*, 6861−6868.
(35) Salloum, D. S.; Schlenoff, J. B. *Biomacromolecules* **2004**, *5*, 1089−1096.
(36) Jackson, M.; Haris, P. I.; Chapman, D. *Biochim. Biophys. Acta* **1989**, *998*, 75−79.
(37) Monsoor, M. A.; Kalapathy, U.; Proctor, A. *Food Chem.* **2001**, *74*, 233−238.
(38) Monsoor, M. A.; Kalapathy, U.; Proctor, A. *J. Agric. Food Chem.* **2001**, *49*, 2756−2760.
(39) Sukhishvili, S. A.; Granick, S. *J. Phys. Chem. B* **1999**, *103*, 472−479.
(40) Sauerbrey, G. *Z. Physik* **1959**, *155*, 206−222.
(41) Höök, F. Ph.D. Thesis Development of a novel QCM technique for protein adsorption studies. 2001. Chalmers University of Technology.
(42) Voinova, M. V.; Rodahl, M.; Jonson, M.; Kasemo, B. *Phys. Scr.* **1999**, *59*, 391−396.
(43) Needs, P. W.; Rigby, N. M.; Ring, S. G.; MacDougall, A. J. *Carbohydr. Res.* **2001**, *333*, 47−58.
(44) Ousalem, M.; Busnel, J. P.; Nicolai, T. *Int. J. Biol. Macromol.* **1993**, *15*, 209−213.
(45) Brant, D. A.; Flory, P. J. *J. Am. Chem. Soc.* **1965**, *87*, 2788−2790.
(46) Marudova, M.; Lang, S.; Brownsey, G. J.; Ring, S. G. *Carbohydr. Res.* **2005**, *340*, 2144−2149.
(47) Ramsden, J. J. *Q. Rev. Biophys.* **1994**, *27*, 41−105.
(48) Glaser, R. W. *Anal. Biochem.* **1993**, *213*, 152−161.
(49) Lahiri, J.; Isaacs, L.; Grzybowski, B.; Carbeck, J. D.; Whitesides, G. M. *Langmuir* **1999**, *15*, 7186−7198.
(50) Picart, C.; Mutterer, J.; Richert, L.; Luo, Y.; Prestwich, G. D.; Schaaf, P.; Voegel, J. C.; Lavalle, P. *Proc. Natl. Acad. Sci. U.S.A.* **2002**, *99*, 12531−12535.
(51) Lavalle, P.; Picart, C.; Mutterer, J.; Gergely, C.; Reiss, H.; Voegel, J. C.; Senger, B.; Schaaf, P. *J. Phys. Chem. B* **2004**, *108*, 635−648.
(52) Ralet, M. C.; Dronnet, V.; Buchholt, H. C.; Thibault, J. F. *Carbohydr. Res.* **2001**, *336*, 117−125.
(53) Picart, C.; Lavalle, P.; Hubert, P.; Cuisinier, F. J. G.; Decher, G.; Schaaf, P.; Voegel, J. C. *Langmuir* **2001**, *17*, 7414−7424.
(54) Picart, C.; Mutterer, J.; Richert, L.; Luo, Y.; Prestwich, G. D.; Schaaf, P.; Voegel, J. C.; Lavalle, P. *Proc. Natl. Acad. Sci. U.S.A.* **2002**, *99*, 12531−12535.

BM0507249